

Ultrafast Charge Separation and Long-Lived Charge Separated State in Photocatalytic CdS–Pt Nanorod Heterostructures

Kaifeng Wu, Haiming Zhu, Zheng Liu, William Rodríguez-Córdoba, and Tianquan Lian*

Department of Chemistry, Emory University, 1515 Dickey Drive, NE, Atlanta, Georgia 30322, United States

S Supporting Information

ABSTRACT: Colloidal semiconductor–metal nanoheterostructures that combine the light-harvesting ability of semiconductor nanocrystals with the catalytic activity of small metal nanoparticles show promising applications for photocatalysis, including light-driven H₂ production. The exciton in the semiconductor domain can be quenched by electron-, hole-, and energy transfer to the metal particle, and the competition between these processes determines the photocatalytic efficiency of these materials. Using ultrafast transient absorption spectroscopy, we show that, in CdS–Pt heterostructures consisting of a CdS nanorod with a Pt nanoparticle at one end, the excitons in the CdS domain dissociate by ultrafast electron transfer (with a half-life of ~ 3.4 ps) to the Pt. The charge separated state is surprisingly long-lived (with a half-life of $\sim 1.2 \pm 0.6$ μ s) due to the trapping of holes in CdS. The asymmetry in the charge separation and recombination times is believed to be the key feature that enables the accumulation of the transferred electrons in the Pt tip and photocatalysis in the presence of sacrificial hole acceptors.

In recent years, a new class of colloidal nanoheterostructures containing both semiconductor nanorods and metallic domains has been prepared.^{1–10} These materials, combining the size-tunable, light-harvesting property of quantum-confined semiconductor nanocrystals with the catalytic activities of small metal nanoparticles, show promising applications for photocatalysis, including light-driven H₂ production. For examples, CdS–Pt nanorod (NR) heterostructures, in which a Pt nanoparticle is grown selectively at one end of a CdS nanorod, can generate H₂ under illumination in the presence of sacrificial electron donors.^{11–14} Upon absorption of light, excitons are generated in the semiconductor NR. As shown in Figure 1a, the excitons can decay by electron-, hole-, and energy transfer to the metallic domain. The generation of H₂ requires the selective transfer of electrons from the semiconductor to the metal while suppressing the charge recombination, hole transfer, and energy transfer pathways. The competition between these pathways determines the photocatalytic quantum efficiency of these heterostructures. To date, the rates of these processes in strongly coupled semiconductor–metal heterostructures have not been determined, and the mechanism for their photocatalytic activity remains unclear. Furthermore, in heterostructures with plasmonic metallic domains, the exciton and plasmon interaction provides an

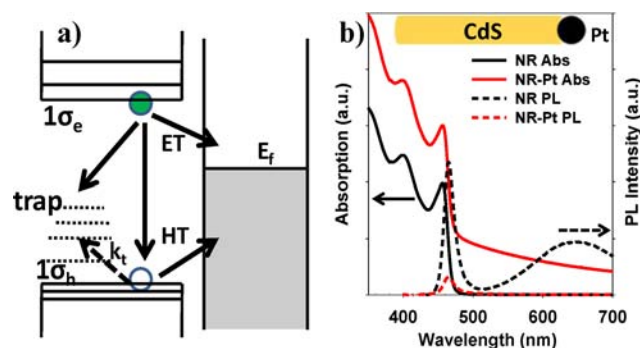


Figure 1. (a) Schematic energy level and exciton quenching pathways in CdS–Pt NR heterostructures. In addition to the intrinsic exciton decay within CdS NRs, the presence of Pt introduces interfacial electron transfer (ET), hole transfer (HT), and energy transfer (not shown) pathways. (b) Absorption (solid lines, left axis) and emission (dashed lines, right axis) spectra of CdS NRs (black) and CdS–Pt NR heterostructures (red). CdS–Pt shows absorption features of both the platinum nanoparticle and CdS NR and significant quenching of band edge and trap state emissions. (Inset) Schematic structure of CdS–Pt.

additional mechanism to control the properties of these “plextonic” nanomaterials.^{15–17}

We choose CdS–Pt NR (inset of Figure 1b) as a model system to investigate the competition of electron, hole, and energy transfer processes in semiconductor–metal heterostructures. Using transient absorption (TA) spectroscopy in conjunction with known molecular electron acceptors, we first identify spectral signatures for the electron, hole, and charge separated state in CdS NRs. Following these spectral signatures, we show that electron transfer from the excited CdS NR to the Pt tip is the main exciton quenching pathway in CdS–Pt. We find that the electron transfer process is ultrafast (~ 3.4 ps) and the charge separated state is surprisingly long-lived ($\sim 1.2 \pm 0.6$ μ s). This slow charge recombination is attributed to ultrafast hole trapping (~ 0.7 ps) in CdS NRs. This finding reveals the mechanism of photodriven H₂ generation in these CdS–Pt NRs and provides insight into the design of NR heterostructures for efficient photocatalysis.

CdS–Pt heterostructures, in which a Pt nanoparticle is grown at one end of a CdS nanorod, were synthesized according to a literature procedure.⁶ TEM images of CdS NRs before and after platinum tips growth (Figure S1, Supporting Information [SI]) indicates an average length of 26.9 ± 2.1 nm

Received: April 5, 2012

Published: June 1, 2012

and diameter of 3.8 ± 0.3 nm for the CdS NR and diameter of 2.3 ± 0.2 nm for the Pt tip. The absorption and photoluminescence (PL) spectra CdS NRs and CdS–Pt are compared in Figure 1b. The CdS NR exhibits discrete transitions arising from quantum confinement in the radial direction.^{18–21} The first absorption peak centered at 456 nm can be attributed to the 1Σ exciton band. In CdS–Pt, the CdS exciton bands remain unchanged (no obvious broadening or shifting), while additional broad absorption features, extending from the UV to near IR, is also observed. The latter can be attributed to the strong d–sp interband transition of platinum nanoparticles.²² PL of CdS NRs shows two distinct emission bands, with a narrow band-edge emission at 463 nm and a broad trap-state emission centered at 650 nm.²³ In CdS–Pt, the trap-state emission is completely quenched, while the band-edge emission is also significantly reduced, indicating a faster decay of electron and/or holes in the excited NR.

In order to reveal the exciton quenching mechanism in CdS–Pt NRs, we use TA spectroscopy to follow the carrier dynamics in CdS and CdS–Pt NRs. The details of the TA spectrometers have been described elsewhere.^{24,25} We first identify the spectral signatures of electrons, holes, and charge separation in CdS NRs. Unlike the well-studied quantum dots (QDs),^{26–32} these spectral signatures in the 1D NRs have yet to be unambiguously assigned.^{33–35} The TA spectra of CdS NRs after 400 nm excitation (Figure 2a) shows a red-shifted

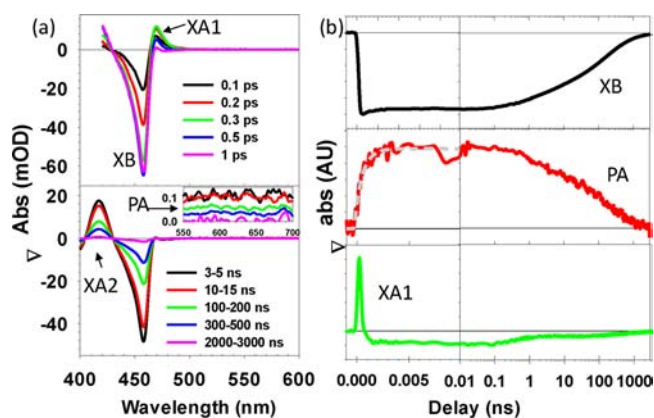


Figure 2. (a) TA spectra of CdS NRs at indicated time delays after 400 nm excitation: 0–1 ps (top) and 3–3000 ns (bottom). (Inset) Expanded view of the broad photoinduced absorption (PA) spectra. (b) TA kinetics for three spectral features: exciton bleach (XB at ~ 456 nm, black line, top), photoinduced absorption (PA from 550 to 700 nm, red line, middle), and hot-exciton induced shift (XA1 at ~ 470 nm, green line, bottom). A fit to the rise of the PA signal (with a single exponential time constant of 0.7 ps) is also shown in the middle panel (gray dashed line).

absorption feature (XA1) at early delay time that decays rapidly (with a time constant of 70 fs) to form a bleach of the 1Σ exciton band (XB) and a derivative-like feature of higher-energy exciton bands (XA2). In addition to these exciton band features, a broad photoinduced absorption band (PA) at wavelength longer than 500 nm is also formed with a rise time of 0.7 ps (Figure 2b, middle panel). These spectral features are remarkably similar to those observed in CdS^{36–38} and CdSe^{28,39–41} QDs and are assigned in the same manner. The XA1 feature at 470 nm can be attributed to hot excitons in the NR, whose presence shifts the 1Σ exciton band to lower energy. The decay of hot carriers to the 1σ orbitals gives rise to the

state-filling-induced bleach of 1Σ XB. Because of the state-specific biexciton interaction energy, this exciton relaxation process also affects the higher energy exciton transitions, giving rise to the growth of the higher-energy XA2 feature and the decrease of XA1 feature. The XA2 feature reflects the interaction of the 1Σ exciton with other exciton bands and can be well described by a red-shift of these transitions (see Figure S3, SI).⁴² The XB feature shows only slight decay ($\sim 16\%$) within 1 ns (Figure 2b), indicating the dominance of the long-lived single exciton state at this excitation intensity.

In CdSe and CdS QDs the XB signal is attributed to the state filling of the electron level with negligible contribution from the hole due to a higher degeneracy of the hole levels.^{30–32} The assignment of the broad PA signal is less clear and has been attributed to both the electron⁴¹ and hole.^{28,36–38} In order to identify the carrier contribution to both XB and PA signals in CdS NRs, known electron acceptors, methyl viologen (MV^{2+}) and benzoquinone (BQ) molecules, are used to selectively remove the excited electrons by interfacial electron transfer. The TA spectra of NR– MV^{2+} complexes (Figure S4, SI) show an ultrafast recovery of the 1Σ XB signal within 100 ps and a corresponding formation of the $MV^{+\bullet}$ radicals absorption band centered at 620 nm and a derivative-like feature of the 1Σ exciton band.⁴¹ These spectral features confirm the ultrafast transfer of electrons from the NR and support the assignment of the XB feature in the CdS NR to the state filling of the 1σ electron level, consistent with the findings of a previous study on CdSe NR– MV^{2+} complexes.³⁴

The overlap of the $MV^{+\bullet}$ radical absorption with the PA signal hinders an unambiguous assignment of the latter. For this reason, we also studied CdS–BQ complexes, in which the reduced BQ anion has negligible absorption in the visible region.⁴³ As shown in Figure 3, the ET process in CdS–BQ complexes leads to a faster recovery of the XB compared to free NRs. However, the ET process does not affect the PA signal, suggesting that the PA signal can be attributed to holes in the NR. The PA signal in NR–BQ complexes decays more slowly

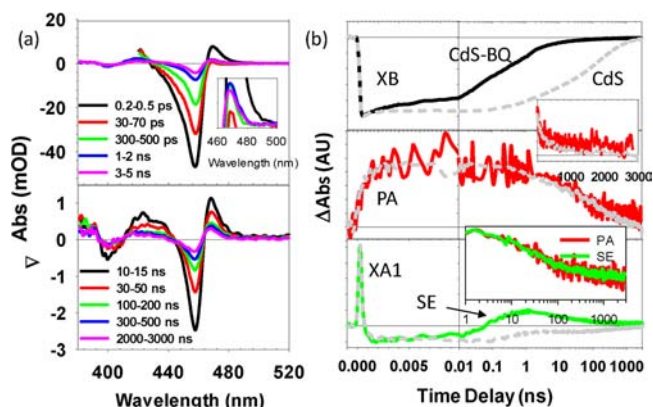


Figure 3. (a) TA spectra of CdS–BQ complexes at indicated delay time windows after 400 nm excitation: 0.2 ps – 5 ns (upper panel) and 10–3000 ns (lower panel). (Inset - upper panel) Formation of charge separation-induced Stark effect signal (SE). (b) TA kinetics for the XB (black solid line, top), PA (red solid line, middle), and XA1 and SE (green solid line, bottom) features in CdS–BQ complexes. In each panel, the kinetics of free CdS NRs (gray dashed line) is also included for comparison. (Inset - middle panel) Expanded view of the comparison of PA kinetics in free NRs and NR BQ complexes. (Bottom) Kinetics for PA and SE signals from 1 to 3000 ns, reflecting the charge recombination process.

than that in free NRs (in the 100–10000 ns time scale, Figure 3b inset), which can be attributed to slow charge recombination in this system. It is interesting to note that the ~ 0.7 ps rise time of PA signal (Figure 2b, middle panel) is similar to the hole trapping time in CdS QDs determined by fluorescence up-conversion measurement,⁴⁴ suggesting the PA signal in the NR is likely due to the trapped holes.^{36–38} Time-resolved PL measurement (Figure S2, SI) shows an ultrafast decay ($\ll 25$ ps) of the band-edge emission and ultrafast formation ($\ll 25$ ps) of the trap-state emission, consistent with the ultrafast trapping of the valence band hole and the small band edge emission quantum yield (0.11%, see SI). Furthermore, the decay of trap-state emission and the XB and PA TA signals follow the same kinetics (Figure S2C, SI), suggesting that the main decay pathway of the 1σ electron is through recombination with the trapped holes in the CdS NR.

In addition to the small PA feature, the TA spectra of the charge separated state of the NR–BQ complexes (>1 ns) show pronounced derivative-like features of the exciton bands that are similar to those observed in the charge separated state of QD–acceptor complexes and can be assigned to the Stark-effect (SE)-induced exciton band shift in the presence of the charge separated pair ($\text{NR}^+ - \text{BQ}^-$).^{24,25} This feature leads to the reappearance of the red-shifted 1Σ and higher-energy exciton bands (SE, Figure 3b, bottom panel) at ~ 1 ns. Although similar to the biexciton-induced shift (XA), the SE feature is much weaker in comparison. The kinetics of the formation of the SE signal and XB recovery agree with each other, supporting the assignment of the SE feature. After 1 ns, the SE signal decays with the same kinetics as that of the PA feature (inset of Figure 3b) due to the charge recombination process. This suggests that both the PA and SE spectral features can be used to follow the charge recombination kinetics, although the latter will be used in the NR–Pt complexes due to its larger signal amplitude.

After the assignment of TA signals of the electron, hole, and charge separated state in CdS NRs, we investigated the exciton quenching mechanism in CdS–Pt NRs. A control experiment of Pt nanoparticles of similar size shows negligible TA spectral signatures in the visible region after 400 nm excitation (Figure S5b, SI). Therefore all TA features in CdS–Pt (Figure 4a) can be attributed to the excitation of the CdS domain. However, due to the absorption of Pt (Figure S5a, SI, and Figure 1), their amplitudes are reduced by a factor of 2 compared to free CdS NRs under the same conditions. The TA spectra of CdS–Pt NRs shows that, in the first 100 ps, the XB feature decays by $\sim 90\%$ while the PA signal displays negligible change, indicating the depopulation of 1σ electrons without the removal of the trapped holes. This suggests that ultrafast electron transfer (with a half-life of ~ 3.4 ps) from the excited CdS NR to the Pt tip is the main exciton quenching pathway.

The 1σ exciton bleach recovery is accompanied by the formation of a derivative-like feature of exciton bands similar to that observed previously in CdS–BQ complexes. The TA spectra can be simulated as a sum of the SE and XB features (Figure S6, SI). The SE signal amplitude is smaller in CdS–Pt, likely reflecting the different dipolar field strength of the charge separated state in these complexes. The simulation also shows that at ~ 3 – 5 ns, the charge separation efficiency in CdS–Pt is near unity. The charge recombination process can be monitored by the decay of the SE signal (Figure 4b), which has a half-life of $1.2 \pm 0.6 \mu\text{s}$. Despite the large uncertainty, it is clear that the rate of recombination is much slower than that of

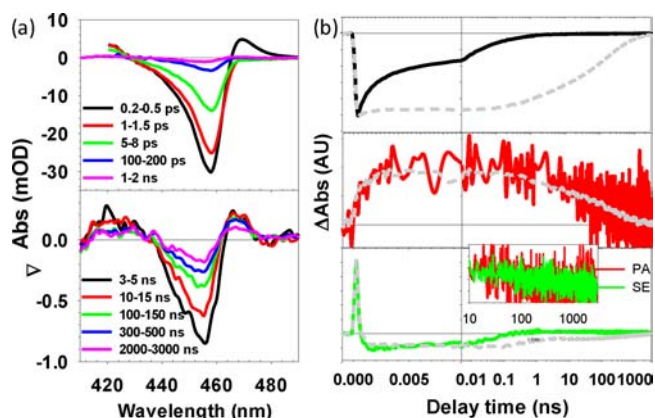


Figure 4. (a) TA spectra of CdS–Pt NRs at indicated time delays: 0.2 ps to 2 ns (upper panel) and 3–3000 ns (lower panel). (b) TA kinetics of XB (black solid line, top), PA (red solid line, middle), and XA1 and SE (green solid line, bottom) spectral features for CdS–Pt NRs. Also shown for comparison are kinetics for CdS NRs (gray dashed lines) at the same wavelengths, whose amplitudes are a factor of 2 larger compared to that of CdS–Pt. (Inset) Comparison of SE and PA kinetics in CdS–Pt after 10 ns.

charge separation. The large difference in these rates is surprising because, as shown in Figure 1a, there exist continua of empty and filled states (above and below the Pt Fermi level, respectively) for both ET and HT from CdS to Pt. The 1σ electron is delocalized in the rod and has considerable overlap with the empty accepting levels in Pt, leading to a fast ET process. The ultrafast trapping of the hole in the CdS reduces its overlap with the filled Pt levels, slowing down the HT process (in the initial exciton state and in the charge separated state). This large difference in the charge separation and recombination rates enables the removal of the trapped hole in the presence of hole acceptors, leading to the accumulation of electrons in the Pt tip and photocatalytic H_2 production.^{13,14} Thus, the hole-trapping-induced asymmetry in the ET and HT times is essential for efficient photoinduced charge separation and photocatalysis in these NR Pt heterostructures. The observed ET rate is much faster than that reported in a previous study of longer (~ 100 nm) CdS–QRs decorated with Pt NPs.¹¹ The reasons for the different ET rates are unclear, and ongoing studies are examining the dependence on the QR length and diameter.

In conclusion, the mechanism of exciton quenching and charge separation in the CdS–Pt NR heterostructure has been investigated by transient absorption spectroscopy. The dominant exciton quenching pathway is ultrafast interfacial ET (~ 3.4 ps) from the CdS NR to the Pt tip. The charge recombination process is surprisingly slow ($\sim 1.2 \pm 0.6 \mu\text{s}$). The asymmetry in the ET and HT rates across the CdS–Pt interface can be attributed to the efficient trapping of the hole in the NR. This asymmetry is essential for efficient accumulation of the transferred electrons in the Pt tip and photocatalysis.

■ ASSOCIATED CONTENT

📄 Supporting Information

Synthesis procedure, TEM images, PL decay kinetics of CdS NRs, TA spectra, and kinetics of CdS– MV^{2+} complexes, TA spectra of Pt, and spectral fitting for CdS, CdS–BQ, and CdS–Pt. This material is available free of charge via the Internet at <http://pubs.acs.org>.

■ AUTHOR INFORMATION

Corresponding Author

tljian@emory.edu.

Funding

This work was funded in part by the U.S. Department of Energy, Office of Basic Energy Sciences, Solar Photochemistry Program (DE-FG02-07ER-15906).

Notes

The authors declare no competing financial interest.

■ REFERENCES

- (1) Mokari, T.; Rothenberg, E.; Popov, I.; Costi, R.; Banin, U. *Science* **2004**, *304*, 1787.
- (2) Mokari, T.; Costi, R.; Sztrum, C. G.; Rabani, E.; Banin, U. *Phys. Status Solidi (b)* **2006**, *243*, 3952.
- (3) Saunders, A. E.; Popov, I.; Banin, U. *J. Phys. Chem. B* **2006**, *110*, 25421.
- (4) Shi, W.; Zeng, H.; Sahoo, Y.; Ohulchanskyy, T. Y.; Ding, Y.; Wang, Z. L.; Swihart, M.; Prasad, P. N. *Nano Lett.* **2006**, *6*, 875.
- (5) Yang, J.; Elim, H. I.; Zhang, Q.; Lee, J. Y.; Ji, W. *J. Am. Chem. Soc.* **2006**, *128*, 11921.
- (6) Habas, S. E.; Yang, P.; Mokari, T. *J. Am. Chem. Soc.* **2008**, *130*, 3294.
- (7) Carbone, L.; Jakab, A.; Khalavka, Y.; Sönnichsen, C. *Nano Lett.* **2009**, *9*, 3710.
- (8) Menagen, G.; Macdonald, J. E.; Shemesh, Y.; Popov, I.; Banin, U. *J. Am. Chem. Soc.* **2009**, *131*, 17406.
- (9) Khon, E.; Hewa-Kasakarage, N. N.; Nemitz, I.; Acharya, K.; Zamkov, M. *Chem. Mater.* **2010**, *22*, 5929.
- (10) Li, X.; Lian, J.; Lin, M.; Chan, Y. *J. Am. Chem. Soc.* **2010**, *133*, 672.
- (11) Berr, M. J.; Vaneski, A.; Mauser, C.; Fischbach, S.; Susha, A. S.; Rogach, A. L.; Jäckel, F.; Feldmann, J. *Small* **2012**, *8*, 291.
- (12) Acharya, K. P.; Khnayzer, R. S.; O'Connor, T.; Diederich, G.; Kirsanova, M.; Klinkova, A.; Roth, D.; Kinder, E.; Imboden, M.; Zamkov, M. *Nano Lett.* **2011**, *11*, 2919.
- (13) Berr, M.; Vaneski, A.; Susha, A. S.; Rodriguez-Fernandez, J.; Doblinger, M.; Jackel, F.; Rogach, A. L.; Feldmann, J. *Appl. Phys. Lett.* **2010**, *97*, 093108.
- (14) Amirav, L.; Alivisatos, A. P. *J. Phys. Chem. Lett.* **2010**, *1*, 1051.
- (15) Manjavacas, A.; Abajo, F. J. G. a. d.; Nordlander, P. *Nano Lett.* **2011**, *11*, 2318.
- (16) Fofang, N. T.; Grady, N. K.; Fan, Z.; Govorov, A. O.; Halas, N. J. *Nano Lett.* **2011**, *11*, 1556.
- (17) von Fofang, N. T.; Park, T.-H.; Neumann, O.; Mirin, N. A.; Nordlander, P.; Halas, N. J. *Nano Lett.* **2008**, *8*, 3481.
- (18) Shabaev, A.; Efros, A. L. *Nano Lett.* **2004**, *4*, 1821.
- (19) Hu, J.; Wang, Li, L.-s.; Yang, W.; Alivisatos, A. P. *J. Phys. Chem. B* **2002**, *106*, 2447.
- (20) Katz, D.; Wizansky, T.; Millo, O.; Rothenberg, E.; Mokari, T.; Banin, U. *Phys. Rev. Lett.* **2002**, *89*, 086801.
- (21) Giblin, J.; Vietmeyer, F.; McDonald, M. P.; Kuno, M. *Nano Lett.* **2011**, *11*, 3307.
- (22) Johnson, R. C.; Li, J.; Hupp, J. T.; Schatz, G. C. *Chem. Phys. Lett.* **2002**, *356*, 534.
- (23) Saunders, A. E.; Ghezelbash, A.; Sood, P.; Korgel, B. A. *Langmuir* **2008**, *24*, 9043.
- (24) Zhu, H.; Song, N.; Lian, T. *J. Am. Chem. Soc.* **2011**, *133*, 8762.
- (25) Zhu, H.; Song, N.; Lian, T. *J. Am. Chem. Soc.* **2010**, *132*, 15038.
- (26) Yang, Y.; Rodríguez-Córdoba, W.; Lian, T. *J. Am. Chem. Soc.* **2011**, *133*, 9246.
- (27) Huang, J.; Huang, Z. Q.; Yang, Y.; Zhu, H. M.; Lian, T. Q. *J. Am. Chem. Soc.* **2010**, *132*, 4858.
- (28) Huang, J. E.; Huang, Z. Q.; Jin, S. Y.; Lian, T. Q. *J. Phys. Chem. C* **2008**, *112*, 19734.
- (29) Huang, J.; Stockwell, D.; Huang, Z. Q.; Mohler, D. L.; Lian, T. Q. *J. Am. Chem. Soc.* **2008**, *130*, 5632.
- (30) Klimov, V. I. *Annu. Rev. Phys. Chem.* **2007**, *58*, 635.
- (31) Boulesbaa, A.; Issac, A.; Stockwell, D.; Huang, Z.; Huang, J.; Guo, J.; Lian, T. *J. Am. Chem. Soc.* **2007**, *129*, 15132.
- (32) Klimov, V. I. *J. Phys. Chem. B* **2000**, *104*, 6112.
- (33) Khon, E.; Mereshchenko, A.; Tarnovsky, A. N.; Acharya, K.; Klinkova, A.; Hewa-Kasakarage, N. N.; Nemitz, I.; Zamkov, M. *Nano Lett.* **2011**, *11*, 1792.
- (34) Jiang, Z.-J.; Kelley, D. F. *J. Phys. Chem. C* **2011**, *115*, 4594.
- (35) Costi, R.; Saunders, A. E.; Elmalem, E.; Salant, A.; Banin, U. *Nano Lett.* **2008**, *8*, 637.
- (36) Baral, S.; Fojtik, A.; Weller, H.; Henglein, A. *J. Am. Chem. Soc.* **1986**, *108*, 375.
- (37) Haase, M.; Weller, H.; Henglein, A. *J. Phys. Chem.* **1988**, *92*, 4706.
- (38) Gopidas, K. R.; Bohorquez, M.; Kamat, P. V. *J. Phys. Chem.* **1990**, *94*, 6435.
- (39) Tyagi, P.; Kambhampati, P. *J. Chem. Phys.* **2011**, *134*, 094706.
- (40) Burda, C.; Link, S.; Mohamed, M.; El-Sayed, M. *J. Phys. Chem. B* **2001**, *105*, 12286.
- (41) McArthur, E. A.; Morris-Cohen, A. J.; Knowles, K. E.; Weiss, E. A. *J. Phys. Chem. B* **2010**, *114*, 14514.
- (42) Sacra, A.; Norris, D. J.; Murray, C. B.; Bawendi, M. G. *J. Chem. Phys.* **1995**, *103*, 5236.
- (43) Burda, C.; Green, T. C.; Link, S.; El-Sayed, M. A. *J. Phys. Chem. B* **1999**, *103*, 1783.
- (44) Klimov, V.; Bolivar, P. H.; Kurz, H. *Phys. Rev. B* **1996**, *53*, 1463.